Spectroscopic investigation of Mn^{2+}, Pr^{3+} codoped $KMgF_3$ under vacuum-ultraviolet excitation

Spectroscopic investigation of Mn^{2+}, Pr^{3+} codoped $KMgF_3$ under vacuum-ultraviolet excitation

Stefan Kück[1,3] **and Irena Sokólska**[2]

[1] Physikalisch-Technische Bundesanstalt, Section 4.13 Bundesallee 100, 38116 Braunschweig, Germany
[2] Not affiliated

E-mail: stefan.kueck@ptb.de

Abstract

Pr^{3+}:$KMgF_3$, Mn^{2+}:$KMgF_3$ and Pr^{3+}, Mn^{2+}:$KMgF_3$ single crystals were grown by the Czochralski method and spectroscopically investigated in order to evaluate possible energy transfer processes between Pr^{3+} and Mn^{2+} after vacuum-ultraviolet excitation. These processes are of importance for the possible use of these materials as phosphors for discharge lamps based on the xenon discharge excitation. In Pr^{3+}:$KMgF_3$ besides the already known cascade emitting Pr^{3+} centre ($^1S_0 \rightarrow \ ^1I_6$, $^3P_0 \rightarrow 4f^2$) (Sokólska and Kück 2001 *Chem. Phys.* **270** 355), a second Pr^{3+} centre was clearly observed with 4f5d energy levels shifted to energies below the $^1S_0$ level. For Mn^{2+}:$KMgF_3$ a broad emission band typical for Mn^{2+} with a maximum at 600 nm and the expected Mn^{2+} excitation bands in the visible ($3d^5 \rightarrow 3d^5$) and vacuum ultraviolet ($3d^5 \rightarrow 3d^44s$) are observed. In the Pr, Mn:$KMgF_3$ sample investigated, the expected energy transfer process $[^1S_0(Pr^{3+}), \ ^6A_1(Mn^{2+})] \rightarrow [(^1I_6, \ ^3P_{0,1,2})(Pr^{3+}), (^4A_1, \ ^4E)(Mn^{2+})]$ could not be observed within the detection limit of the experimental setup. The efficiency for this energy transfer process was also calculated assuming dipole–dipole interaction and found to be $<5\%$ for the sample investigated. The low concentration of the dopant ions and the small oscillator strength of the $^6A_1 \rightarrow (^4A_1, \ ^4E)$ transition of the Mn^{2+} acceptor ion is responsible for this low transfer efficiency.

1. Introduction

The Pr^{3+} ion could be a suitable activator ion for phosphors for Xe discharge lamps, because in some materials it exhibits a cascade emission process. This means that after an excitation with a high energetic photon from, e.g., synchrotron radiation or Xe discharge, it emits more

[3] Author to whom any correspondence should be addressed.
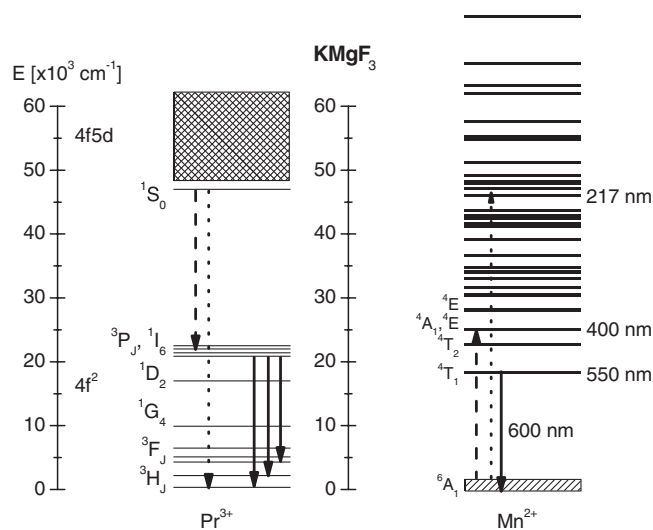
Figure 1. Energy level schemes of Pr^{3+} and Mn^{2+} in $KMgF_3$. The dashed and dotted lines indicate possible nonradiative energy transfer processes.

than one photon in the visible spectral range. For Pr^{3+}, this phenomenon was observed for the first time for $Pr^{3+}:YF_3$ [2–4]. The high energetic excitation brings about a cascade emission due to the two-step intraconfigurational $4f^2$–$4f^2$ transitions: $^1S_0 \rightarrow {}^1I_6$ (approx. 400 nm) followed by $^3P_0 \rightarrow {}^3H_{4,5,6}$, $^3F_{2,3,4}$ (approx. 480–720 nm). The presence of such a two-photon emission in Pr^{3+}-doped materials was also observed in $NaYF_4$ [2, 3], $NaLaF_4$ [4], LaF_3 [5], $KMgF_3$ [1], $LiCaAlF_6$ and $LiSrAlF_6$ [6], PrF_3 [7], $BaMgF_4$ and LuF_3 [8], $LaZrF_7$ and $LaZr_3F_{15}$ [9], $BaSiF_6$ [10], $SrAl_{12}O_{19}$ [11], $LaMgB_5O_{10}$ [12] and LaB_3O_6 [13]. Recently, the structural characteristics of a host material in which photon cascade emission occurs have been understood in general [14–16], so that a purposeful search for new and efficient cascade emitters is possible.

For $Pr^{3+}:KMgF_3$, photon cascade emission was observed with an estimated quantum efficiency of 1.24 for the spectral range of 400–750 nm [1]. However, the photon in the first step of this cascade ($\sim$400 nm) cannot be used directly for application because of the low sensitivity of the human eye at this wavelength. Thus, transfer partner ions for Pr^{3+} have to be found to convert the energy of this 400 nm photon into a photon at an energy more suitable for fluorescent lamps. In YF_3, the rare earth ions Sm^{3+}, Eu^{3+}, Dy^{3+}, Er^{3+} and Tm^{3+} were investigated; however, despite resonant transitions, energy transfer was not observed [17]. In Er^{3+} codoped $Pr^{3+}:CaAl_{12}O_{19}$ crystals, Wang *et al* observed a transfer efficiency from the Pr^{3+} $^1S_0$ level to the Er^{3+} ion of up to 25% [18]. Also Mn^{2+} appears to be a suitable transfer partner ion, because it exhibits a resonant transition ($^6A_1 \rightarrow {}^4A_1$, ^4E) for the Pr^{3+} $^1S_0 \rightarrow ({}^1I_6$, $^3P_{0,1,2}$) transition (see figure 1). In this paper we report on the results of the spectroscopic investigation of the codoped Mn, $Pr:KMgF_3$ system and give an analysis of the energy transfer processes between Pr^{3+} and Mn^{2+} after vacuum-ultraviolet (VUV) excitation.

2. Experimental details

The $KMgF_3$ samples singly doped with Mn^{2+} (2 at.%) and Pr^{3+} (0.75 at.%) as well as codoped with both Mn^{2+} (2 at.%) and Pr^{3+} (1 at.%) were grown by the Czochralski method.

The concentrations given are nominal concentrations in the melt. For Mn^{2+} a distribution coefficient close to unity is expected for the substitution on the Mg^{2+} site; however, for Pr^{3+} the distribution coefficient is much lower. From the spectroscopic data reported in [1], it is assumed that the Pr^{3+} ion favourably enters the $KMgF_3$ lattice on the K^+ site, despite the large differences in the ion radii ($r(Pr^{3+}) = 143$ pm, $r(K^+) = 174$ pm for the 12-fold-coordination [19]) and in the valences. A substitution for the Mg^{2+} cannot be excluded ($r(Mg^{2+}) = 86$ pm in six-fold coordination), but in MgF_2 incorporation of Pr^{3+} was not observed [7]. However, as will be seen in this paper, a second Pr^{3+} centre is also clearly observed. This observation is in accordance with the results reported by Francini *et al* [20] for Ce^{3+}:$KMgF_3$, where two Ce^{3+} centres were observed. One site is the K^+ substitutional site with perfect cubo-octahedral O_h symmetry and the other one is the same site with two perturbing K^+ vacancies, which lower the local symmetry to orthorhombic C_{4v} [20].

The spectroscopic investigation were mostly carried out at the SUPERLUMI station of HASYLAB (Hamburger Synchrotron Laboratorium) at DESY (Deutsches Elektronen-Synchrotron) in Hamburg. For details of the experimental setup see [21]. The experiments were performed at room temperature (RT). The spectral range of the excitation measurements was 50–350 nm (24.7–3.5 eV) with a resolution of 0.3 nm. The excitation spectra were not corrected for the photon flux of the excitation beam, because this is not relevant for the investigation performed within this study. The emission spectra were measured with two setups. In the 200–300 nm range a 0.5 m monochromator and a Solarblind (Hamamatsu) photomultiplier were used. In the 300–600 nm spectral range a 0.5 m monochromator and a XP2020Q photomultiplier were used. The resolutions are given in the corresponding figure captions. For both setups the correction curves were not available at the time of the experiments. The kinetics of the emission decays were measured by a standard single-photon counting method. The determination of the decay of the emission is limited by the period of 192 ns between the synchrotron radiation bunches. The duration of a synchrotron pulse is approximately 130 ps.

The excitation measurements in the spectral region between 250 and 600 nm were carried out at the Institute of Laser-Physics at the University of Hamburg. A commercial Jobin-Yvon Fluorolog III system was used with a xenon lamp placed in front of a 0.25 m monochromator as the excitation source and a R-928P photomultiplier placed behind a 0.25 m monochromator as the detection system.

3. Experimental results and discussion

3.1. Mn^{2+}:$KMgF_3$

Figure 2(a) shows the emission and excitation spectra of Mn^{2+}:$KMgF_3$. The emission is due to the $^4T_1 \rightarrow {}^6A_1$ transition. It is typical for the Mn^{2+} ion in octahedral coordination and covers the orange to red spectral region between 550 and 700 nm. Thus, this emission is suitable for lighting applications. The excitation spectrum exhibits the typical Mn^{2+} transitions between the $^6A_1$ ground state and the $3d^5$ excited states (see figure 1). The $^6A_1 \rightarrow ({}^4A_1, {}^4E)$ transition around 400 nm is resonant to the $Pr^{3+}{}^1S_0 \rightarrow ({}^1I_6, {}^3P_{0,1,2})$ emission transition. The strong excitation bands between 180 and 155 nm are tentatively assigned to transitions into the 4s bands of the Mn^{2+} ion [22, 23].

3.2. Pr^{3+}:$KMgF_3$

Figure 2(b) shows the emission and excitation spectra of singly Pr^{3+} doped $KMgF_3$. The spectra have already been discussed in detail in [1] and exhibit the typical $4f^2 \rightarrow 4f^2$ and $4f^2 \rightarrow 4f5d$ transition bands (see also the energy level scheme depicted in figure 1).
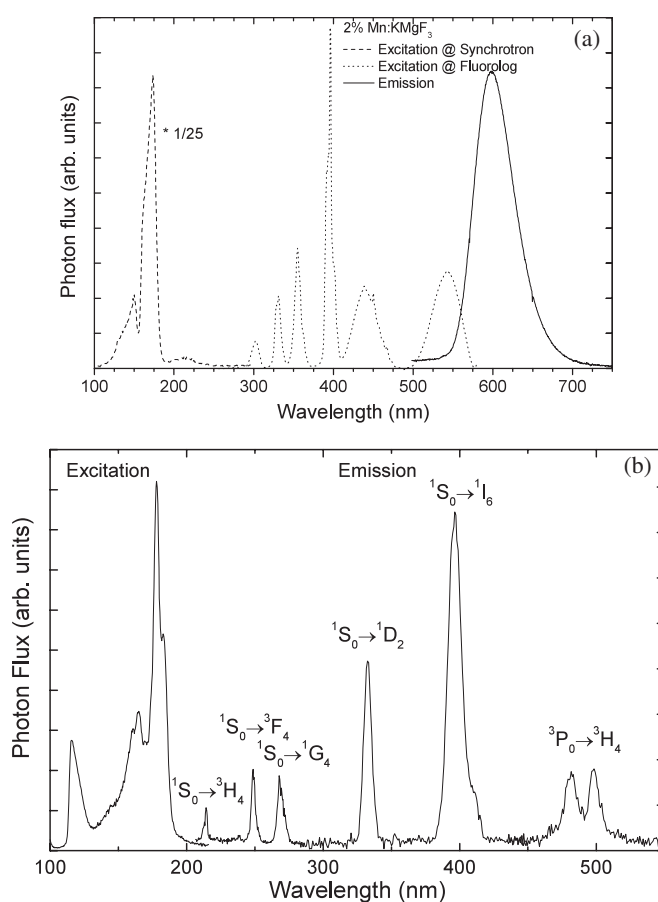
Figure 2. (a) Mn^{2+}:$KMgF_3$, room temperature emission spectrum excited at 173.5 nm and excitation spectra monitored at 600 nm. (b) Pr^{3+}:$KMgF_3$ (PCE-centre), room temperature emission spectrum excited at 178 nm and excitation spectra monitored at 396 nm.

Besides this already identified Pr^{3+} centre with cascade emission [1] ('PCE-centre'), we also observed a second Pr^{3+} centre. In figure 3(a) the emission spectrum of Pr^{3+}:$KMgF_3$ is shown for an excitation at 195 nm and—for comparison—for excitation at 179 nm. In the first spectrum the first step of the cascade is not observed, but the emission transitions from the $^3P_0$ level. Compared to the emission transitions from the $^3P_0$ level from the PCE-centre, the emission lines are at different wavelengths. This is especially pronounced for the $^3P_0 \rightarrow {}^3H_4$ transition, located at 499 nm for the second centre and at 488 nm for the PCE-centre. The weak emission signal around 400 nm in the emission spectrum of the second centre is assumed to be caused by a residual absorption into the 4f5d levels of the PCE-centre. Emission bands due to 4f5d $\rightarrow$ 4f^2 transitions are not observed, mainly due to nonradiative multiphonon quenching into the (^3P_J, $^1I_6$) levels. Also the excitation spectrum for a detection wavelength of 499 nm differs from that for a detection wavelength of 397 nm (see figure 3(b)). Broad excitation bands due to 4f5d transitions are observed for both centres, but at considerably different spectral positions. The excitation peaks of the lowest energetic 4f5d band are shifted from 183 to 204 nm (corresponding to approximately 5625 cm^{-1}) for the second centre. Thus for this centre the 4f5d level is energetically below the $^1S_0$ level. For Ce^{3+}:$KMgF_3$ also, two centres
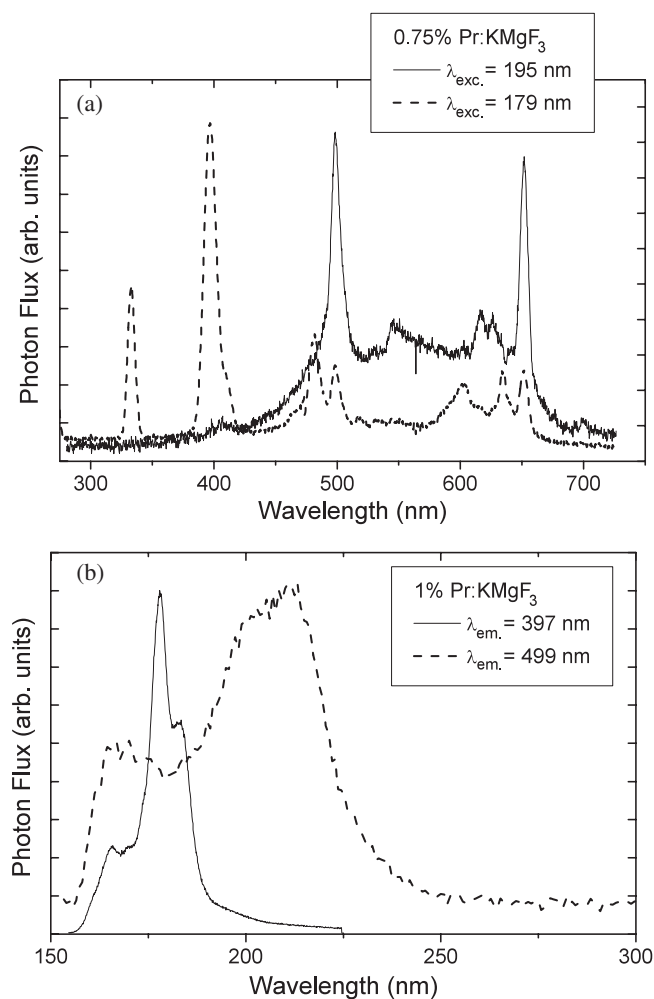
Figure 3. (a) Emission spectra of Pr^{3+}:$KMgF_3$ excited at 195 nm (second centre) and 179 nm (PCE-centre), normalized to the same height. (b) Excitation spectra of Pr^{3+}:$KMgF_3$ monitored at 499 nm (second centre) and 397 nm (PCE-centre), normalized to the same height.

for the Ce^{3+} ion were observed, with wavelengths for the lowest 5d levels at about 234 and 272 nm, corresponding to energies of 42 735 and 36 765 cm^{-1}, respectively, for the Ce^{3+} ion on the O_h-site and on the C_{4v}-site, respectively [20]. According to the detailed investigation of Dorenbos [24, 25] the energetic position $E(Pr^{3+}, 4f5d)$ of the lowest 4f5d level of Pr^{3+} can be calculated from the lowest energy $E(Ce^{3+}, 5d)$ of the 5d level of Ce^{3+} as follows:

$$E(Pr^{3+}, 4f5d) = E(Ce^{3+}, 5d) + 12\,240\ cm^{-1} \pm 750\ cm^{-1}. \tag{1}$$

Thus, the Pr^{3+} levels are expected to be at energies of 54 975 $cm^{-1} \pm 750\ cm^{-1}$ for the O_h site and at 49 005 $cm^{-1} \pm 750\ cm^{-1}$ for the C_{4v} site, respectively. These values are in good agreement with the experimental results. The lowest 4f5d bands of Pr^{3+} in $KMgF_3$ are found at approximately 54 645 cm^{-1} (corresponding to 183 nm) and 49 020 cm^{-1} (corresponding to 204 nm) (see figure 3(b)).
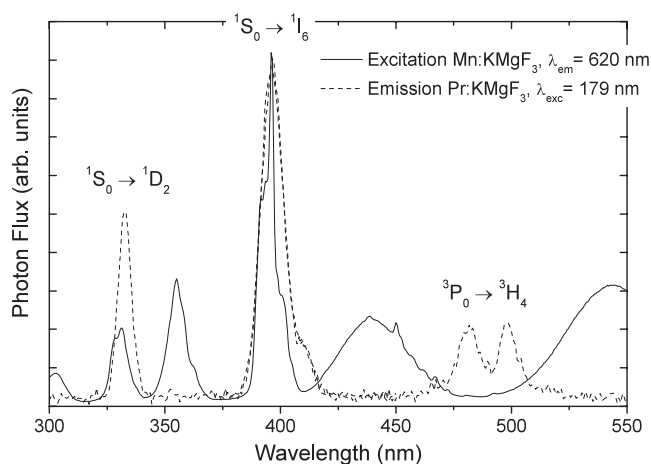
Figure 4. Room temperature emission spectrum of Pr^{3+}:$KMgF_3$ and excitation spectrum of Mn^{2+}:$KMgF_3$ indicating the good spectral overlap between Pr^{3+} $^1S_0$ emission bands and Mn^{2+} excitation bands between 330 and 410 nm.
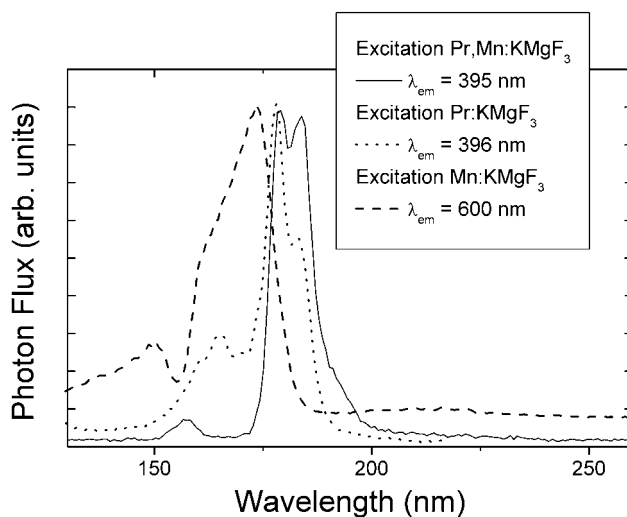
Figure 5. Excitation spectra of Pr^{3+}:$KMgF_3$, Mn:$KMgF_3$ and Pr, Mn:$KMgF_3$ normalized to the same height.

3.3. Pr^{3+}, Mn^{2+}:$KMgF_3$

The excitation spectrum of the Mn^{2+} emission and the emission spectrum of the Pr^{3+} PCE-centre are shown in figure 4. The overlap is very good, especially for the bands at 330 and 400 nm. Thus in principle an efficient energy transfer should be possible, and we investigated possible energy transfer processes within the Pr^{3+}, Mn^{2+}:$KMgF_3$ system.

In figure 5 the excitation spectra of Pr:$KMgF_3$ and Pr, Mn:$KMgF_3$ for a monitor wavelength of ~395 nm (Pr^{3+} $^1S_0 \rightarrow {}^1I_6$ transition) are shown. The 4f5d bands of Pr^{3+} are clearly observed in both spectra; however, their shapes differ. From a comparison with the Mn^{2+} excitation spectrum (monitored at 600 nm, also shown in figure 5), we explain this
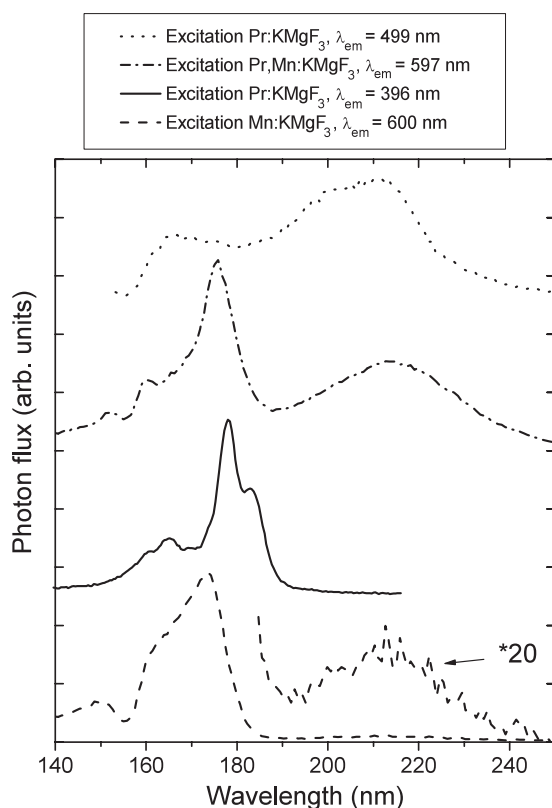
Figure 6. Excitation spectra of $Mn:KMgF_3$ (dashed line) and Pr, $Mn:KMgF_3$ (dashed–dotted line) for a monitoring wavelength of $\sim$600 nm (Mn^{2+}) and excitation spectra of $Pr:KMgF_3$ for the second Pr^{3+} centre (dotted line) and PCE-centre of Pr^{3+} (solid line), monitored at 499 and 396 nm. The spectra are shifted in y and are normalized to the same height.

change in the shapes with a competing absorption of the excitation radiation into the Mn^{2+} 4s bands in the wavelength range between approximately 150 and 180 nm. (Note especially the pronounced structure at 157.5 nm, which occurs as a dip in the 600 nm excitation spectrum of $Mn^{2+}:KMgF_3$ and as a band in 395 nm excitation spectrum of Pr^{3+}, $Mn^{2+}:KMgF_3$.) If there were to be a transfer from the 4s levels of Mn^2 to the 4f5d levels of Pr^{3+}, the Mn^{2+} excitation bands should also be seen in the excitation spectrum of the Pr^{3+} $^1S_0 \rightarrow$ $^1I_6$ transition at 395 nm in the Pr, $Mn:KMgF_3$ sample. However, due to the small energy gaps between the excited Mn^{2+} levels it is expected that the excitation into the Mn^{2+} ion will decay via multiphonon relaxation into the metastable state, i.e. $^4T_1$. This relaxation occurs fast compared to a possible transfer to the Pr^{3+} ion.

In figure 6 the excitation spectra of $Mn:KMgF_3$ (dashed line) and Pr, $Mn:KMgF_3$ (dashed–dotted line) for a monitoring wavelength of $\sim$600 nm (Mn^{2+}) are shown. The broad excitation band between 190 and 250 nm appears in both spectra. However, the intensity ratio between this band and the 4s excitation bands of Mn^{2+} between 140 and 180 nm is much higher for the Pr, $Mn:KMgF_3$ sample. We assume two things are responsible for this observation: first, the excitation into the second Pr^{3+} centre (shown as dotted line) could be transferred to the Mn^{2+} and thus add to the excitation. Second, the excitation into the PCE-centre of Pr^{3+} (shown as a solid line) competes with the Mn^{2+} excitation bands and thus diminishes the excitation into the
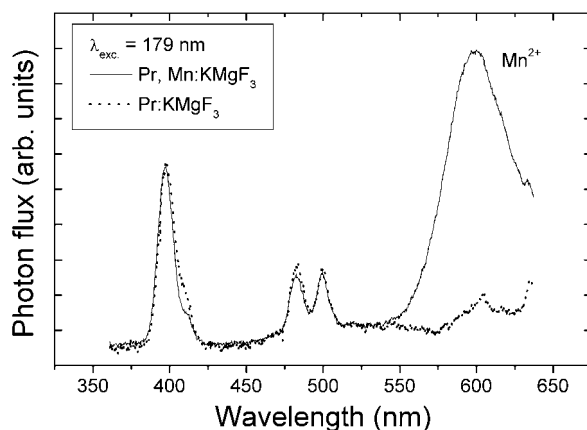
Figure 7. Emission spectra of Pr^{3+}:$KMgF_3$ and Pr^{3+}, Mn^{2+}:$KMgF_3$ for an excitation wavelength of 179 nm. The spectra are scaled to the 400 nm band.

Mn^{2+} band in the spectral region between 175 to 190 nm. From these observations we conclude that an energy transfer between the Pr^{3+} 4f5d levels of the PCE-centre and the $Mn^{2+}3d^5$ levels would be very weak, if it occurs at all. This means that the samples investigated are not suitable for phosphor application, at least not with the concentrations investigated.

In figure 7 the emission spectra of Pr^{3+}:$KMgF_3$ and Pr^{3+}, Mn^{2+}:$KMgF_3$ for an excitation wavelength of 179 nm are shown. For Pr^{3+}, Mn^{2+}:$KMgF_3$ in addition to the Pr^{3+} emission bands at 400, 488 and 499 nm, the Mn^{2+} emission band is also observed. However, this is not a verification for energy transfer, because at 179 nm the Mn^{2+} ion is also excited (see figure 2(a)). However, in case of transfer, the ratio between the 400 and 488 nm emission band of Pr^{3+} should change in favour of the 488 nm band. Although the latter band is slightly higher in the spectrum, it is not proof for an energy transfer.

The decay characteristic of the Mn^{2+} emission ($\sim$ms-range) shows no evidence of a rise time, which should be observed in the case of a $Pr^{3+} \rightarrow Mn^{2+}$ energy transfer (the lifetime of the $^1S_0$ level is in the $\sim\mu$s range).

In conclusion, we cannot verify energy transfer between Pr^{3+} and Mn^{2+} in the $KMgF_3$ lattice, at least not for the experimental conditions and concentrations used in this study. However, the discussion above also shows that the verification of energy transfer between Mn^{2+} and Pr^{3+} is difficult, because of overlapping transitions.

4. Calculation of energy transfer efficiency

The transfer efficiency η_T between a donor and an acceptor can be described by

$$\eta_T = \frac{W_{DA}}{W_r + W_{DA}}, \tag{2}$$

where W_{DA} is the transfer rate between the donor and the acceptor and W_r is the radiative decay rate of the donor. In this simple formula other decay channels like, e.g., multiphonon relaxation and transfer to other acceptors or defect centres, are neglected. The radiative decay rate is related to the oscillator strength f_D of the emission transition as follows [26]:

$$W_r = \frac{[1/3(n^2 + 2)]^2 n}{1.5 \times 10^4 \text{ s m}^{-2}} \cdot \frac{f_D}{\lambda^2} = \frac{c_2}{\lambda^2} f_D, \tag{3}$$

where $n \approx 1.404$ (at 589.3 nm) [27]) is the refractive index, $\lambda \approx 400$ nm is the emission wavelength and $c_2 = 1.64 \times 10^{-4}$ m^2 s^{-1} for $KMgF_3$. The energy transfer rate W_{DA} can be described in the electric dipole–dipole interaction according to Dexter [28]:

$$W_{DA} = \left(\frac{1}{4\pi\varepsilon_0}\right)^2 \frac{3\hbar e^4 \lambda^2}{4\pi n^4 c^2 m^2} \frac{1}{R^6} f_D f_A \beta \int g_D(E)g_A(E)\,dE$$
$$= c_1 \frac{\lambda^2}{R^6} f_D f_A \beta \int g_D(E)g_A(E)\,dE \tag{4}$$

where $c_1 = 4.61 \times 10^{-48}$ m^4 J s^{-1} for $KMgF_3$, m is the electron mass, R is the distance between the donor and the acceptor, f_A and f_D are the acceptor and donor oscillator strengths and β is the branching ratio of the $^1S_0 \rightarrow (^1I_6, {}^3P_{0,1,2})$ transition, defined as

$$\beta = \frac{\Phi(^1S_0 \rightarrow {}^3P_{0,1,2}, {}^1I_6)}{\Phi(^1S_0 \rightarrow 4f^2)}, \tag{5}$$

where Φ is the photon flux and g_D and g_A are the lineshape functions of the donor emission and acceptor absorption; the integral thus takes into account the spectral overlap. Substituting the equations (4) and (3) into (2) one obtains:

$$\eta_T = \frac{c_1 \frac{\lambda^2}{R^6} f_D f_A \beta \int g_D(E)g_A(E)\,dE}{\frac{c_2}{\lambda^2} f_D + c_1 \frac{\lambda^2}{R^6} f_D f_A \beta \int g_D(E)g_A(E)\,dE} = \frac{1}{1 + \frac{c_2}{c_1} \frac{R^6}{f_A \lambda^4 \beta \int g_D(E)g_A(E)\,dE}}. \tag{6}$$

Thus, the radiative decay rate does not play any role in the transfer efficiency. However, if there are many emission transitions of the donor, only the overlapping spectral part contributes to the transfer process. This is considered here by the branching ratio β. For $KMgF_3$, $\beta \approx 60\%$ [1]. (Note that we neglected here the branching ratio of the $^1S_0 \rightarrow {}^1D_2$ transition of Pr^{3+} (approx. 15% [1]) and its spectral overlap with the $^6A_1 \rightarrow Mn^*$ transition of Mn^{2+}.) Furthermore we assume an optimum spectral overlap, i.e. the absorption lineshape of the Mn^{2+} $(^6A_1 \rightarrow {}^4A_1, {}^4E)$ transition is considered to be identical to the $^1S_0 \rightarrow {}^1I_6$ emission lineshape. Thus:

$$\int g_D(E)g_A(E)\,dE = 4.21 \times 10^{19} \frac{1}{J} \tag{7}$$

and for $KMgF_3$ we finally obtain:

$$\eta_T = \frac{1}{1 + c_3 \cdot \frac{R^6}{f_A}}, \tag{8}$$

with $c_3 = 5.49 \times 10^{49}$ m^{-6}. For Mn^{2+}, the oscillator strength f_A of the $(^6A_1 \rightarrow {}^4A_1, {}^4E)$ transition is typically between 1×10^{-8} and 1×10^{-7} (see e.g. [29]). For our calculation we use $f_A \approx 1 \times 10^{-7}$. Figure 8 shows a plot of the efficiency of the $[^1S_0(Pr^{3+}), {}^6A_1(Mn^{2+})] \rightarrow [(^1I_6, {}^3P_{0,1,2})(Pr^{3+}), ({}^4A_1, {}^4E)(Mn^{2+})]$ energy transfer as a function of the donor–acceptor distance. For an energy transfer efficiency $>50\%$, the acceptor–donor distances have to be less than 3.5 Å; for an efficiency above the estimated detection limit of approximately 5%, the distances have to be less than 6 Å. In $KMgF_3$, the nearest K–Mg distance is 3.455 Å and the second nearest distance is 6.615 Å [30]. Thus, for detectable (and efficient) transfer, the nearest Mg shell has to be occupied by Mn, which is rather unlikely for the low concentrations used in this study.

For the above calculation and estimation of the energy transfer efficiency only electric–dipole interaction was taken into account. This is of course too simple a view of the energy transfer processes. However, if additional transfer processes like magnetic dipole or electric quadrupole interaction or exchange and superexchange interaction occur, than these energy
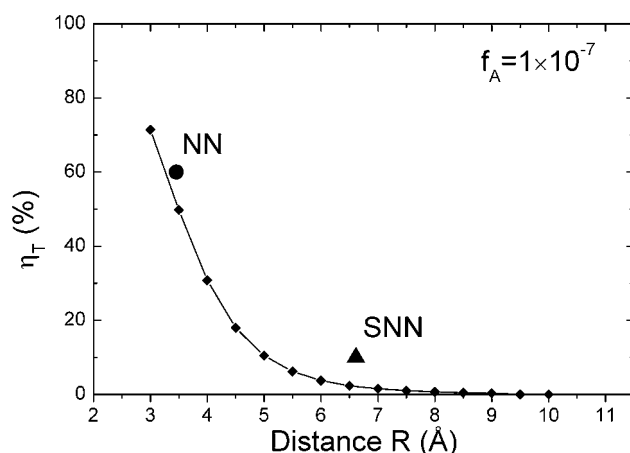
Figure 8. Calculated efficiency of the $[^1S_0(Pr^{3+}), {}^6A_1(Mn^{2+})] \rightarrow [(^1I_6, {}^3P_{0,1,2})(Pr^{3+}),$ $(^4A_1, {}^4E)(Mn^{2+})]$ energy transfer for an acceptor oscillator strength of 1×10^{-7} as a function of the donor–acceptor distance in $KMgF_3$. The nearest Pr^{3+}–Mn^{2+} and second nearest Pr^{3+}–Mn^{2+} distance are also indicated as NN and SNN, respectively.

transfer processes would enhance the energy transfer efficiency calculated with our simple model. In our experiments, we do not observe transfer, thus we assume that in our sample these effects appear also not to be efficient, at least not for the concentrations in our samples.

The transfer efficiency could be enhanced using higher dopant concentrations. In the case of $KMgF_3$, however, an increase in the Pr^{3+} concentration leads to the incorporation of PrF_3, caused by the low solubility of Pr^{3+} in the $KMgF_3$ lattice [1, 7, 15]. An increase in the Mn^{2+} concentration is certainly possible, because the compound $KMnF_3$ exists. However, in this case, there would be a strong absorption into the high-lying Mn^{2+} excitation bands followed by a fast relaxation into the metastable $^4T_1$ level. Thus, in conclusion, $KMgF_3$ seems not to be a suitable host material with respect to the realization of a Pr^{3+}–Mn^{2+}-based phosphor useful for VUV excitation.

5. Summary

Pr^{3+}, Mn^{2+} and Pr^{3+}, Mn^{2+} doped $KMgF_3$ crystals were grown and spectroscopically investigated. Typical Mn^{2+} and Pr^{3+} excitation and emission spectra were observed in the singly doped samples. A second Pr^{3+} centre was found. In the codoped sample the energy transfer process $[^1S_0(Pr^{3+}), {}^6A_1(Mn^{2+})] \rightarrow [(^1I_6, {}^3P_{0,1,2})(Pr^{3+}), (^4A_1, {}^4E)(Mn^{2+})]$ could not be observed. The transfer efficiency for this process was analysed in general based on electric dipole–dipole interaction. Calculations show that the energy transfer efficiency is expected to be small for Mn^{2+} due to the small oscillator strength of the $^6A_1 \rightarrow (^4A_1, {}^4E)$ transition. In conclusion, for a Pr^{3+}–Mn^{2+}-based phosphor to be used in Xe discharge lamps $KMgF_3$ is not a suitable host material.

Acknowledgments

References

[1] Sokólska I and Kück S 2001 *Chem. Phys.* **270** 355
[2] Sommerdijk J L, Bril A and de Jager A W 1974 *J. Lumin.* **8** 341
[3] Sommerdijk J L, Bril A and de Jager A W 1974 *J. Lumin.* **9** 288
[4] Piper W, de Luca J A and Ham F S 1974 *J. Lumin.* **8** 344
[5] Levey C G, Glynn T J and Yen W M 1984 *J. Lumin.* **31/32** 245
[6] Kück S and Sokólska I 2002 *J. Electrochem. Soc.* **149** J27
[7] Kück S and Sokólska I 2003 *Appl. Phys.* A **77** 469
[8] Kück S and Sokólska I 2002 *Chem. Phys. Lett.* **364** 273
[9] van der Kolk E, Dorenbos P and van Eijk C W E 2001 *Opt. Commun.* **197** 317
[10] van der Kolk E, Dorenbos P, van Eijk C W E, Vink A P, Fouassier C and Guillen F 2002 *J. Lumin.* **97** 212
[11] Srivastava A M and Beers W W 1997 *J. Lumin.* **71** 285
[12] Srivastava A M, Doughty D A and Beers W W 1996 *J. Electrochem. Soc.* **143** 4113
[13] Srivastava A M, Doughty D A and Beers W W 1997 *J. Electrochem. Soc.* **144** L190
[14] Rodnyi P A, Mikhrin S B, Dorenbos P, van der Kolk E, van Eijk C W E, Vink A P and Avanesov A G 2002 *Opt. Commun.* **204** 237
[15] Kück S, Sokólska I, Henke M, Döring M and Scheffler T 2003 *J. Lumin.* **102/103** 176
[16] Kück S, Sokólska I, Henke M, Scheffler T and Osiac E 2005 *Phys. Rev.* B **71** 165112
[17] Zachau M, Zwaschka F and Kummer F 1998 *Proc. 6th Int. Conf. Luminescent Materials* ed C R Ronda and T Welker (Pennington: Electrochemical Society) p 314
[18] Wang X J, Huang S, Lu L, Yen W M, Srivastava A M and Setlur A A 2001 *Opt. Commun.* **195** 405
[19] Kaminskii A A 1981 *Laser Crystals* (*Springer Series in Optical Sciences* vol 14) (Berlin: Springer) ISBN: 3-540-09576-4
[20] Francini R, Grassano U M, Landi L, Scacco A, D'Elena M, Nikl M, Cechova N and Zema N 1997 *Phys. Rev.* B **56** 15109
[21] Zimmerer G 1991 *Nucl. Instrum. Methods Phys. Res.* A **308** 178
[22] Sabatini J F, Salwin A E and McClure D S 1975 *Phys. Rev.* B **11** 3832
[23] True M 2004 *Dissertation* Universität Hamburg, Institut für Experimentalphysik (http://www.sub.uni-hamburg.de/opus/volltexte/2004/2254)
[24] Dorenbos P 2000 *J. Lumin.* **91** 91
[25] Dorenbos P 2000 *J. Lumin.* **91** 155
[26] Henderson B and Imbusch G F 1989 *Optical Spectroscopy of Inorganic Solids* (Oxford: Clarendon)
[27] Uchino K, Nomura S, Vedam K, Newnham R E and Cross L E 1984 *Phys. Rev.* B **29** 6921
[28] Dexter D L 1953 *J. Chem. Phys.* **21** 836
[29] Ferguson J, Guggenheim H J and Tanabe Y 1965 *J. Appl. Phys.* **36** 1046
[30] *Inorganic Crystal Structure Database, Fachinformationszentrum Karlsruhe* www.fiz-karlsruhe.de